Roles of conserved basic amino acid residues and activation mechanism of the hyperthermophilic aspartate racemase at high temperature. Proteins

ARTICLE *in* PROTEINS STRUCTURE FUNCTION AND BIOINFORMATICS · AUGUST 2006

Impact Factor: 2.63 · DOI: 10.1002/prot.21010 · Source: PubMed

7 AUTHORS, INCLUDING:

Okimasa Okada
Mitsubishi Tanabe Pharma Corporation
19 PUBLICATIONS **227** CITATIONS
SEE PROFILE

Lijun Liu
University of California, San Francisco
24 PUBLICATIONS **729** CITATIONS
SEE PROFILE

Masafumi Yohda
Tokyo University of Agriculture and Techno…
215 PUBLICATIONS **4,080** CITATIONS
SEE PROFILE

PROTEINS: Structure, Function, and Bioinformatics 64:502–512 (2006)

Roles of Conserved Basic Amino Acid Residues and Activation Mechanism of the Hyperthermophilic Aspartate Racemase at High Temperature

Takumitsu Yoshida,[1] Tomohiro Seko,[2] Okimasa Okada,[2] Kousuke Iwata,[1] Lijun Liu,[3] Kunio Miki,[3] and Masafumi Yohda[1,*]

[1]*Department of Biotechnology and Life Science, Tokyo University of Agriculture and Technology, Tokyo, Japan*
[2]*Technology and Development, Fuji Xerox Co., Ltd., Kanagawa, Japan*
[3]*Department of Chemistry, Graduate School of Science, Kyoto University, Kyoto, Japan*

ABSTRACT **X-ray crystallography has revealed two similar α/β domains of the aspartate racemase from the hyperthermophilic archaeon, *Pyrococcus horikoshii* OT3. The active site is located in the cleft between the two domains where two cysteine residues face each other. This arrangement allows the substrate to enter the cleft and enables the two cysteine residues to act synergistically. However, the distance between their thiolates was estimated to be 9.6 Å, which is beyond the distance for cooperative action of them. We examined the molecular mechanism for the racemization reaction of this hyperthermophilic aspartate racemase by mutational analyses and molecular dynamics simulations. The mutational analyses revealed that Arg48 and Lys164 were essential for catalysis in addition to the putative catalytic cysteine residues. The molecular dynamics simulations revealed that the distance between the two active γ-sulfur atoms of cysteine residues oscillate to periodically become shorter than the predicted cooperative distance at high temperature. In addition, the conformation of Tyr160, which is located at the entrance of the cleft and inhibits the entry of a substrate, changes periodically to open the entrance at 375 K. The opening of the gate is likely to be induced by the motion of the adjacent amino acid, Lys164. The entrance of an aspartate molecule was observed by molecular dynamics (MD) simulations driven by the force of the electrostatic interaction with Arg48, Lys164, and also Asp47. These results provide insights into the roles of amino acid residues at the catalytic site and also the activation mechanism of a hyperthermophilic aspartate racemase at high temperature. Proteins 2006;64:502–512.** © 2006 Wiley-Liss, Inc.

Key words: aspartate racemase; D-amino acid; molecular dynamics simulation; hyperthermophilic; docking simulation

INTRODUCTION

Although the L-enantiomers of amino acids are predominant in living organisms, the D-enantiomers are also distributed ubiquitously in eubacteria as components of peptidoglycan in cell walls. In recent years, D-amino acids were also found in archaea, invertebrates, and mammals.[1–3] D-Ser in the mammalian brain functions as a mediator or transmitter in the mammalian nervous and endocrine systems.[4] There exist high concentrations of D-aspartate in several hyperthermophilic archaea.[1] High concentrations of D-aspartate and aspartate racemase were also found in blood shell *Scapharca broughtonii* (Mollusca) tissues.[5] However, the functions of D-amino acids in archaea and invertebrates are still unclear.

D-amino acids are usually endogenous and, in most cases, amino acid racemases (AARs) are responsible for their biosynthesis. All known AARs are thought to employ a mechanism that involves deprotonation at the α-carbon atom of the substrate amino acid, followed by reprotonation of the resulting carbanionic intermediate from the reverse side and in turn inversion of the configuration.[6] AARs can be divided into two classes, pyridoxal 5′-phospate (PLP)–dependent and independent types.[7] AspR belongs to the PLP-independent group along with glutamate racemase (GluR) and employs a two-base mechanism to catalyze racemization.[8] These enzymes utilize cysteine residues as the conjugated catalytic acid and base.[9–13]

We have determined the three-dimensional structure of *Pyrococcus horikoshii* OT3 AspR (PhAspR) by X-ray crystallography at a resolution of 1.9 Å.[14] The monomer of PhAspR consists of two compact α/β domains, which are

Abbreviations: AAR, amino acid racemases; AspR, aspartate racemase; GluR, glutamate racemase; PhAspR, aspartate racemase from *Pyrococcus horikoshii* OT3; DAAO, D-amino acid oxidase from porcine kidney, LAAO, L-aspartic acid oxidase from *Pyrococcus horikoshii* OT3; SDS-PAGE, sodium dodecyl sulfate - polyacrylamide gel electrophoresis; MD, molecular dynamics; RMSD, root-mean-square displacement; PCA, principal component analysis.

Takumitsu Yoshida, Tomohiro Seko, and Okimasa Okada contributed equally to this work.

Lijun Liu's present address is Institute of Molecular Biology, Howard Hughes Medical Institute and Department of Physics, University of Oregon, Eugene, OR 97403.

*Correspondence to: Masafumi Yohda, Department of Biotechnology and Life Science, Tokyo University of Agriculture and Technology, 2-24-16 Naka-cho, Koganei, Tokyo, 184-8588, Japan. E-mail: yohda@cc.tuat.ac.jp

Received 5 January 2005; Revised 28 February 2006; Accepted 1 March 2006

Published online 16 May 2006 in Wiley InterScience (www.interscience.wiley.com). DOI: 10.1002/prot.21010

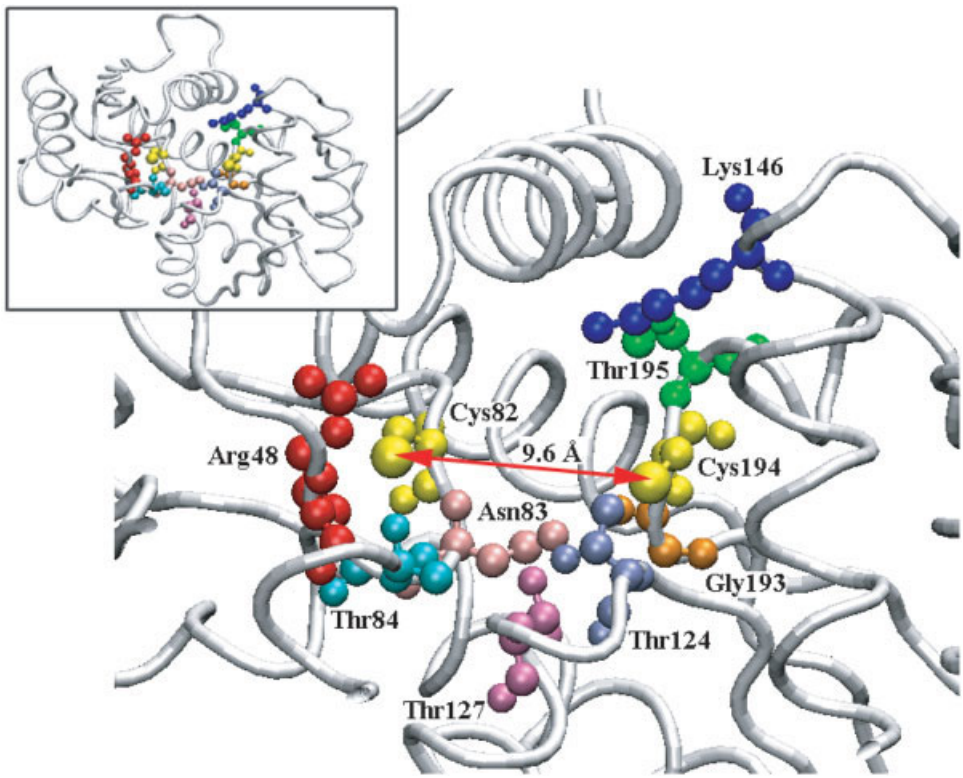

Fig. 1. The structure of the catalytic site of PhAspR. The backbone is drawn by tube model, and the putative catalytic important amino acid residues (Arg48, Cys82, Asn83, Thr84, Thr124, Thr127, Lys164, Gly193, Cys194, and Thr195) are shown by ball and stick model. The arrow designates the distance between two catalytic cysteine residues. The inset represents the whole molecular structure of PhAspR.

highly homologous. The N-terminal domain is composed of residues 1 to 102 and 214 to 228, and the C-terminal domain includes residues 103 to 213. The C-terminal helix α13 folds back into the N-terminal, forming a hinge with a large cleft between the two domains. The putative active site of this enzyme is located in the cleft between the two domains, where two cysteine residues (Cys82 and Cys194) face each other (Fig. 1). This arrangement allows the substrate to enter the cleft and enables the two cysteine residues to act synergistically as the catalytic base/acid pair, to abstract/donate a proton from/to the α-carbon site of the substrate/intermediate.

Among the residues located at the active center, besides the conserved fragments of Cys82Asn83Thr84 and Gly193Cys194Thr195, Arg48 and Lys164 are strictly conserved in all AspRs. In addition, Thr124 and Thr127 are also conserved in both AspRs and GluRs. In the present structure, Arg48 and Thr84 are located around Cys82, and Lys164 and Thr124 around Cys194. Interestingly, the spatial arrangement of these residues is quasi mirror-symmetrical (Fig. 1). The residues of Arg48/Lys164, with a positively charged long side-chain, can ionically interact with the side-chain carboxylate of L-/D-Asp via its guanidinium/ammonium group, and Thr84/Thr124 can form a hydrogen bond with the amino or positively charged ammonium group of L-/D-Asp. This characteristic structure may play crucial roles in the positioning and orientating of substrates and should be associated with the symmetric nature of racemization. This triad structure composed of Cys, Thr, and Arg/Lys might be responsible for the stereoselectivity of chirality.

We have expressed the C-terminal domain and found that it took almost the same structure as the wild type.[15] However, it did not exhibit any racemizing activity for either L- or D-aspartic acids, suggesting that synergetic cooperation between the two sides is indispensable for the racemization reaction. As the transition state of proton transfer between two atoms is essentially a hydrogen bond interaction,[16] the proton transfer in the process of aspartate racemization will proceed through the approximate distance of two hydrogen bonds. Thus, the cooperative distance between the α-sulfur atoms of the two active cysteine residues could be assigned as ~ 8.0 Å, twice the sulfur-involved hydrogen bond distance.[17] However, the experimentally observed distance between the two α-sulfur atoms of the active cysteine residues is 9.6 Å. At such a distance, cooperation between the two cysteine residues is probably difficult. Because *Pyrococcus horikoshii* is a hyperthermophilic archaeon preferring a temperature of 98°C, a so-called hinge motion between two domains could be responsible for narrowing the cleft to drive the synergetic behavior at high temperature. The putative catalytic two cysteine residues in *Aquifex* GluR are located in each domain and are separated by about 7.6 Å, which is much shorter than 9.6 Å.[18] Even so, the distances between them and the α-carbon of D-Gln, a substrate analogue, were not

short enough for deprotonation and protonation. Thus, it is postulated that they should be within a proximal distance in the real glutamate racemase and substrate complex.

In this study, we performed mutation analyses and molecular dynamics simulations to elucidate the molecular mechanism for the racemization reaction of a hyperthermophilic aspartate racemase.

MATERIALS AND METHODS

Materials and Enzymes

D-amino acid oxidase from porcine kidney (DAAO) was purchased from Biozyme Laboratories (South Wales, UK). A plasmid for expressing L-aspartic acid oxidase from *Pyrococcus horikoshii* OT3 (LAAO) was kindly provided by Professor Toshihisa Ohshima of Tokushima University.[19] LAAO was purified by heat treatment at 70°C for 30 min and hydrophobic chromatography using Butyl-Toyopearl 650M (Tosoh, Tokyo, Japan). Horseradish peroxidase was a product of Wako Pure Chemical Industries (Osaka, Japan). 4-aminoantipyrine and *N*-ethyl-*N*-(2-hydroxy-3-sulfopropyl)-*m*-toluidine were obtained from Dojindo Laboratories (Kumamoto, Japan). D, L-aspartic amino acid and all other reagents were of the highest grade available and solutions were made up in ultra pure water.

Plasmid Construction and Mutant Purification

Plasmids coding for PhAspR single point mutants (C82A, C194A, R48I, R48K, R48A, N83G, T84A, T124A, T127A, K164L, K164R, K164A) were prepared from pPH0670E[20] with the QuikChange Site-Directed Mutagenesis Kit (STRATAGENE, La Jolla, CA) using the following primers (C82A Fw 5′-TAA-TAA-TGC-CGG-CTA-ACA-CCG-CG-3′,Rv 5′-CGC-GGT-GTT-AGC-CGG-CAT-TAT-TA-3′; C194A, 5′-Fw TAA-TAG-CTG-GCG-CTA-CCG-AAG-TT-3′, Rv 5′-AAC-TTC-GGT-AGC-GCC-AGC-TAT-TA-3′; N83G, Fw 5′- AAT-AAT-GCC-TTG-TGG-TAC-CGC-GCA-TGC-GT-3′, Rv 5′- ACG-CAT-GCG-CGG-TAC-CAC-AAG-GCA-TTA-TT-3′;T84A, 5′-TGT-AAC-GCC-GCA-CAT-GCG-TTT-GT-3′, 5′-ACA-AAC-GCA-TGT-GCG-GCG-TT-ACA-AGG-CA-3′; T124A, Fw 5′-TGG-CTT-GCT-AGC-GGC-CAC-TGG-AAC-TAT-A-3′, Rv 5′- TAT-AGT-TCC-AGT-GGC-CGC-TAG-CAA-GCC-A-3′; T127A, Fw 5′- TGC-TAC-TAC-TGG-CGC-CAT-AGT-GAG-TGG-A-3′, Rv 5′- TCC-ACT-CAC-TAT-GGC-GCC-AGT-AGT-AGC-A-3′; R48I, Fw 5′- CAA-ATT-CCT-GAT-ATC-ACT-GCT-TAT-ATT-CTT-3′, Rv 5′- AAG-AAT-ATA-AGC-AGT-GAT-ATC-AGG-AAT-TTG-3′; R48A, Fw 5′- CAA-ATT-CCT-GAT-GCA-ACT-GCT-TAT-ATT-3′, Rv 5′- AAT-ATA-AGC-AGT-TGC-ATC-AGG-AAT-TTG-3′; R48K Fw 5′- CTC-AAA-TTC-CTG-ATA-AAA-CTG-CTT-ATA-TTC-3′, Rv 5′- GAA-TAT-AAG-CAG-TTT-TAT-CAG-GAA-TTT-GAG-3′; K164L, Fw 5′- TAT-GAG-GGG-GTT-TTG-GCC-GGG-AAT-TTG-3′, Rv 5′-CAA-ATT-CCC-GGC-CAA-AAC-CCC-CTC-ATA-3′, K164A, Fw 5′- TAT-GAG-GGG-GTT-GCG-GCC-GGG-AAT-TTG-3′, Rv 5′- CAA-ATT-CCC-GGC-CGC-AAC-CCC-CTC-ATA-3′; K164R, Fw 5′- TAT-GAG-GGG-GTT-CGA-GCC-GGG-AAT-TTG-3′, Rv 5′- CAA-ATT-CCC-GGC-TCG-AAC-CCC-CTC-ATA-3′). All constructs were verified by DNA sequencing. These mutant proteins were expressed in *Escherichia coli*, and were purified in the same manner as the wild-type enzyme.[20]

Assay for Aspartate Racemase Activity

The kinetic constants for purified wild-type and mutant PhAspRs in both the L- → D-Asp and D- → L-Asp reactions were determined. The racemase reaction mixtures (100 μL) containing various concentrations of L- (or D-) Asp in 10 m*M* Tris-HCl, pH 8.0 (at 25°C), were incubated in the presence of wild-type or mutant PhAspRs at 70°C. The reaction mixtures were mixed with 200 μL of 20 m*M* 4-aminoantipyrine, 20 m*M* *N*-ethyl-*N*-(2-hydroxy-3-sulfopropyl)-*m*-toluidine, 0.12 unit of DAAO (or approximately 100 μg of LAAO), and 2 units of horseradish peroxidase, and then incubated at 37°C (or 50°C) for 30 min. Thereafter, the condensation product was quantified by measuring the absorbance at 555 nm using a Microplate Reader Model 550 (Bio-Rad). Additionally, the amount of enantiomer produced by PhAspR during the specific oxidase reaction was determined and subtracted.

For the analyses of racemization activities of C82A and C194A mutants, the amount of enantiomer produced was quantified by HPLC.[21] The reaction was stopped by the addition of ethanol to 70%. After removal of the denatured protein by centrifugation, the supernatant was dried up in vacuo. Then, aspartic acids were dissolved in boric acid buffer (0.2*M* boric acid and 4 m*M* EDTA 2Na, pH 8.0) and derivatized with NBD-F, a fluorogenic derivatizing reagent. Subsequently, enantiomers of aspartate derivatives were separated by HPLC on a Pirkle-type chiral column (Sumichiral OA2500S, Sumika Chemical Analysis Service, Osaka, Japan) and the proportion of D- or L-aspartic acid was determined.

Molecular Dynamics Simulations

The X-ray crystallographic structure of PhAspR (PDB code: 1JFL) is used as the initial structure. Because PhAspR forms a dimer in the crystal structure, the first monomer in the PDB file was taken to prepare the initial structure for molecular dynamics (MD) simulations. Missing atoms in the X-ray crystallographic structure were appropriately added using the LEaP module in a molecular simulation package, AMBER.[22]

One PhAspR molecule was solvated into a spherical water droplet with a radius of 40 Å, where the total number of atoms is 24,160. The solvent water molecules within 1.0 Å of the atoms of PhAspR were removed to avoid close atomic contacts. Because the positions of counter ions are unknown, we did not add any ions to neutralize the MD systems. A half-harmonic potential[22] was applied around the spherical water droplet to prevent the water molecules from evaporating.

The ff96 parameter[23,24] in the AMBER force field along with the TIP3P water model[25] was used in this study. The van der Waals and electrostatic interactions were calculated using a MD Engine II PC (NEC Corporation, Japan), a computer designed for MD calculation. The electrostatic interactions of all atom pairs were calculated without using the cut-off method.[26] A cut-off distance of 15 Å was applied to evaluate the van der Waals interactions.

TABLE I. Kinetic Parameters of Mutant PhAspRs

	L → D Direction			D → L Direction		
WT	Km (m*M*)	k_{cat} (min^{-1})	k_{cat}/Km	Km (m*M*)	k_{cat} (min^{-1})	k_{cat}/Km
WT	1.3×10^{-1}	1.9×10^{4}	1.5×10^{5}	3.1×10^{-1}	2.6×10^{4}	8.4×10^{4}
C82A	1.8	4.0×10^{-1}	2.2×10^{-1}	3.6	1.6×10^{-1}	4.5×10^{-2}
C194A	1.3	9.3×10^{-1}	7.3×10^{-1}	4.5×10^{-1}	1.4×10^{-1}	3.0×10^{-1}
R48I	3.0×10^{2}	1.0×10^{2}	3.5×10^{-1}	4.0×10	6.8	1.7×10^{-1}
R48K	2.3×10	5.5×10^{2}	2.4×10	3.3	5.8×10	1.8×10
R48A	N.D.	N.D.	N.D.	1.5×10^{2}	1.1×10	7.7×10^{-2}
K164L	4.3	2.8×10	6.6	5.4	2.6×10	4.9
K164R	1.0×10^{2}	4.1×10	4.1×10^{-1}	3.1×10	1.1×10	3.4×10^{-1}
K164A	2.3×10^{2}	1.0×10	4.6×10^{-2}	8.7×10	2.9	3.3×10^{-2}
N83G	3.9	2.4×10^{4}	6.1×10^{3}	1.8	7.8×10^{3}	4.3×10^{3}
T84A	8.2×10^{-2}	9.0×10^{2}	1.1×10^{4}	2.6×10^{-1}	1.6×10^{3}	6.0×10^{3}
T124A	1.8×10^{-1}	1.8×10^{3}	9.7×10^{3}	3.2×10^{-1}	1.5×10^{3}	4.7×10^{3}
T127A	1.4×10^{-1}	3.5×10^{3}	2.4×10^{4}	1.6×10^{-1}	3.5×10^{3}	2.2×10^{4}

K_M and k_{cat} values of mutant PhAspRs for L- and D- aspartate at 70°C are shown. N.D.: Not determined.

At first, the potential energy minimization of the initial MD system was carried out using the conjugated gradient method. Under the restrained condition that only the water molecules were allowed to move and the protein was kept frozen, MD simulations were started at 100 K for 200 ps using the energy-minimized structure. The system was equilibrated by gradually increasing the temperature from 100 to 250 K for 400 ps in total, where all atoms were allowed to move. After the equilibration, the system was heated up to 300 and then 350, 375, and 400 K for 1.5 ns at each temperature and at 425 K for 3 ns. An additional 3.5-ns run was performed for detailed analyses at 375 K, which is close to the enzymatically optimal temperature of PhAspR. The trajectories of the atoms above 300 K were stored every 1 ps. VMD[27] was used for the analyses of structure and molecular motion, and for the preparation of graphic representations.

Docking Molecular Dynamics Simulation

The structure of PhAspR at 800 ps in the MD simulation at 375 K was used as the initial structure for docking MD simulations because the phenol group gate was open at this moment. The PhAspR and one L-aspartic acid, which was placed 10 to 25 Å away from the sulfur atoms of cysteine residues in the active site of PhAspR, were solvated into a water box, where the total number of atoms is ~ 44,000. The solvent water molecules within 1.0 Å of the solute atoms were removed and counter ions were not added. The total number of atoms in the system varied with the initial arrangements of PhAspR and the L-aspartic acid. The three-dimensional periodic boundary condition was applied. The particle mesh Ewald method[28,29] was used to calculate the electrostatic interactions. This calculation was performed using LINUX PCs. An integration time step of 2 fs for the equations of motion was used with the SHAKE algorithm.[30] The temperature of the systems was regulated by using Berendsen's method.[31] After the equilibration runs for 100 ps in total below 350 K, the system was heated up to 375 K to observe the behavior of the L- aspartic acid.

Principal Component Analysis

We employed the principal component analysis (PCA)[32–34] to investigate the slow hinge motion. Collective motions in proteins have been investigated by PCA using MD trajectories. After removal of translational and rotational motions, the variance–covariance matrix (σ_{ij}) of fluctuation of the three-dimensional coordinates q_i ($i = 1 \sim 3N; N = 228$) of the α-carbon atoms is calculated by

$$\sigma_{ij} = \langle (q_i - \langle q_i \rangle)(q_j - \langle q_j \rangle) \rangle$$

where $\langle\ \rangle$ represents the time average. The eigenvalues and eigenvectors are obtained by diagonalizing the variance–covariance matrix. The mode with largest eigenvalue corresponds to the slowest mode of molecular motion.

RESULTS

Kinetic Analyses of PhAspR Mutants

As shown in Figure 1, the active site consists of two pseudo mirror-symmetric moieties (Cys82/Thr84/Arg48 and Cys194/Thr124/Lys164). Because the distance between the thiolates of Cys82 and Cys194 is too large for functional cooperation in the deprotonation and protonation of the α-carbon of the substrate, aspartic acid, we have hypothesized that each moiety functions independently of each enantiomer. However, the C-terminal domain did not exhibit any racemase activity for the enantiomers in despite that it retained almost the same conformation as the whole crystal structure.[15] In order to elucidate the PhAspR reaction mechanism, we have examined the catalytic kinetics of the mutated PhAspRs with substitutions of amino acid residues constituting the catalytic site (Table I).

The mutation of either Cys82 or Cys194 to alanine (C82A/C194A) markedly reduced the reaction rate but only marginally affected the K_M constant. These mutants did not show any specificity in either reaction direction, which suggests cooperation between the two cysteine residues. Arg48 was replaced with alanine, isoleucine, or lycine, and Lys164 was replaced with alanine, leucine, or

arginine. In spite of our expectation that mutants with the basic amino acids would exhibit relatively strong activity, all mutations severely impaired the activity. All mutants showed a significant decrease in k_{cat} as compared with the wild-type enzyme, but the effects were relatively small as compared with Cys82A and Cys194A. Therefore, both Arg48 and Lys164 are important but not indispensable for catalysis.

In comparison with other mutants, R48K exhibits relatively strong catalytic activity as well as substrate affinity, suggesting that the positively charged residue of R48 contributes to both the substrate binding and reaction rate of PhAspR. Also, K164A had the weakest activity of the K164 mutants, and K164L had a significantly lower K_M than other mutants of R48 and K164. This result suggests that not only the charge but also the size of the side chain at the 164th position is related to the binding of both aspartate enantiomers to PhAspR.

Other mutations (N83G, T84A, T124A, and T127A) also affected the activity, especially k_{cat} (Table 1). Even so, the effects were marginal compared with mutations at Cys82, Cys194, Arg48, and Lys164. Thus, we think that Asn83, Thr84, Thr124, and Thr127 are not essential for catalysis.

We determined the crystal structures of several mutants prepared in this study (manuscript in preparation). Because the structures are almost the same as that of the wild type, the changes of catalytic activity are not caused by the structural disorder and reflect the roles of mutated amino acids.

Distance between Two Catalytic γ-Sulfur Atoms in Cysteine Residues

Although Cys82 and Cys194 are thought to be responsible for the racemization of aspartic acid, the distance between their γ-sulfur atoms is 9.6 Å, which is far longer than the putative cooperative distance, 8 Å.[14] We speculated that a so-called hinge motion between the two domains, the deformation of two loops containing the two cysteine residues, and the distortion of the two cysteine residue side-chains would help to reduce the distance. To test this hypothesis, MD simulations of PhAspR were performed in a wide temperature range from 300 to 425 K, and the temperature dependence of the intramolecular motion was investigated.

Time evolutions of the root-mean-square displacement (RMSD) at 300 and 425 K of the whole simulated structures from the initial crystal structure are shown in Figure 2. At 300 K, RMSD of the entire protein was lower than ~ 2.3 Å, indicating that the simulated structure was stable [Fig. 2(A)]. The temperature was gradually increased from 300 to 425 K to avoid destabilizing the simulated structure. RMSD at 425 K remained about 2.5 Å during the simulation [Fig. 2(B)]. The structure of PhAspR appears to be stable at the elevated temperature in our MD simulations, and no remarkable unfolded or damaged fragments are observed. This is probable because the hyperthermophilic aspartate racemase is extremely stable and also the simulation was performed with no cutoff method and a long relaxation simulation time using the high-speed calculation accelerator during the steps of increasing temperature.

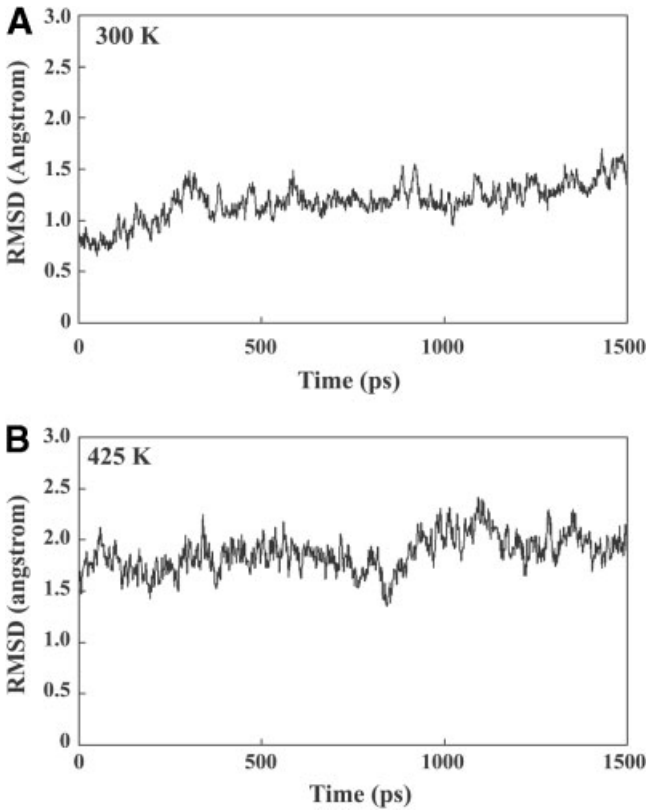

Fig. 2. RMSD of all atoms during the MD simulations. RMSDs of whole atoms of the MD simulated structures at (**A**) 300 K and (**B**) 425 K from the crystal structure were plotted from 0 to 1500 ps.

We analyzed the time evolution of the distance between two catalytic γ-sulfur atoms at 300, 375, 400, and 425 K (Fig. 3). At 300 K, the distance remained around 10.5 Å, even longer than the distance (9.6 Å) in the crystal structure at 90 K, during the simulation [Fig. 3(A)]. At 375 K the distance often decreased to less than 8 Å, which is the optimal cooperative distance assigned for racemization, although the average values was still ~ 11 Å [Fig.3(B)]. A noticeable change in the time evolution of the distance was observed in the simulation at 400 K. The distance decreased from 13 to 9 Å in the first 300 ps, and then increased up to 13 Å in the next 300 ps [Fig. 3(C)]. The observed contraction and expansion of the distance between the two γ-sulfur atoms was more remarkable at 425 K. During the simulation time range from 500 to 1000 ps, the distance decreased from 10 to 6 Å, and then increased up to 10 Å [Fig. 3(D)]. The exact conformation of the two active sulfur atoms located in the cleft was illustrated in images of the molecular structure (Fig. 4). At 680 ps, the two γ-sulfur atoms approached each other to the distance of 5.8 Å [Fig. 4(A)]. The distance is much smaller than the predicted cooperation distance (8.0 Å), suggesting that the aspartate racemization probably proceeds through proton transfer via the cooperation of closer sulfur atoms and that the α-carbon of aspartate may not be colinear with the two γ-sulfurs. In contrast, at 940 ps, the two active sulfur atoms were separated from each other by a distance of up

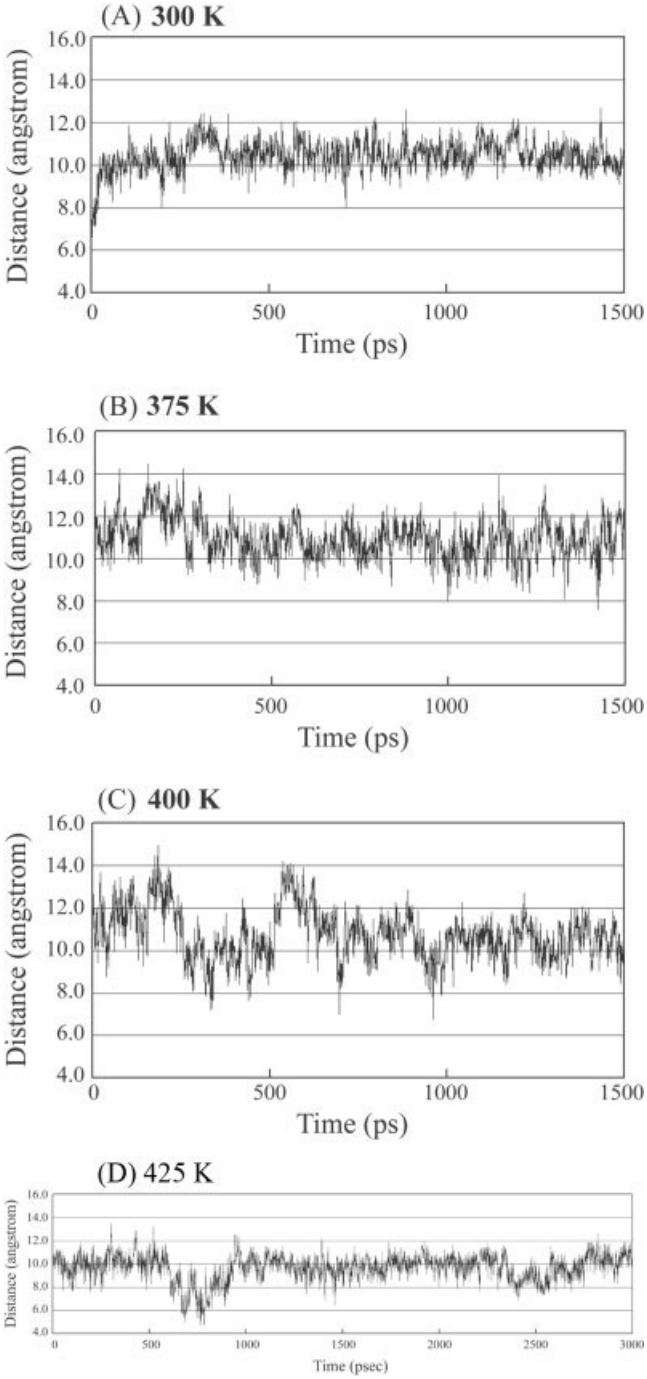

Fig. 3. Time evolution of the distance between two catalytic γ-sulfur atoms during MD simulations. The distance between two catalytic γ-sulfur atoms of active cysteine residues during MD simulations at (**A**) 300 K, (**B**) 375 K, (**C**) 400 K, and (**D**) 425 K are plotted from 0 to 1500 or 3000 ps.

to 10.4 Å, which is even longer than the distance in the crystal structure [Fig. 4(B)]. A similar oscillation of the distance was observed from 2300 to 2800 ps.

The active and inactive states for racemization were observed alternately in the simulation at high temperature, 425 K. Such a description synchronizes with the temperature-driven hinge motion that induces conditions for racemization only when the cleft narrows. A detailed analysis of the conformational change is needed using the result at 375 K, which is close to the physiological optimal temperature for PhAspR. Using the trajectories of α-carbon atoms obtained by MD simulations, the PCA was performed to investigate the slow molecular motion at 375 K. A stereoview of the first mode, which corresponds to the slowest molecular motion, is shown by using a tube model in Figure 5. The slowest mode clearly shows the hinge motion to widen the cleft. This hinge motion might assist the reduction in the distance between the two γ-sulfur atoms of the cysteine residues.

Mechanism for Reducing the Distance between the Two γ-Sulfur Atoms

The distance between the two γ-sulfur atoms in cysteine residues of the X-ray structure is ~ 9.6 Å, which is longer than the assigned distance of 8 Å for the racemization.[14] Liu and colleagues have implied that the reduction in the distance is due to the cooperative hinge motion, the deformation of the loops with the active cysteine residues, and the distortion of the side-chains of cysteine residues.[14] Our simulations showed that the distance was shortened frequently to 8 Å above 375 K for a very short period of time. The PCA showed that the cooperative hinge motion was greatly enhanced above 375 K. The torsional conformational change of the side-chains of the cysteine residues occurred at ~ 350 K. However, conformational change of the backbone in the loop regions was not observed at 375 K. These results showed that the hinge motion and the distortion of the side-chains observed at 375 K would be mainly responsible for the reduction in the distance between the two γ-sulfur atoms.

Phenol Group of TYR160 Is a Gate at the Catalytic Site

In the crystal structure, the bulky phenol group of TYR160 is located just above the active site, possibly blocking the entrance of aspartic acid into the active site. We investigated the motion of the phenol group of TYR160. Time evolutions of two dihedral angles at the side-chain of TYR160, Cα-Cβ-Cγ-Cδ and N-Cα-Cβ-Cγ, are shown in Figure 6. The former dihedral angle varied frequently even at low temperature, which corresponds to the conformational changes due to the rotation of the phenol ring around the central Cβ–Cγ axis. In contrast, the latter dihedral angle did not change at up to 350 K. However, it changed several times during 5 ns at 375 K. This motion leads to a large positional change of the phenol group of TYR160 to blocking or release the blocking of the active site of PhAspR. We speculate that the phenol group operates as the gate of the active site, causing it to be temperature dependent. The dihedral angle N-Cα-Cβ-Cγ in the closed state corresponds to −60° and that in the open state to 180°.

We analyzed the accessible space of the active sites in a closed state at 300 K and in an open state at 375 K using a probe sphere with a radius of 1 Å. The grid points with intervals of 0.1 Å are shown as black points in Figure 7. In

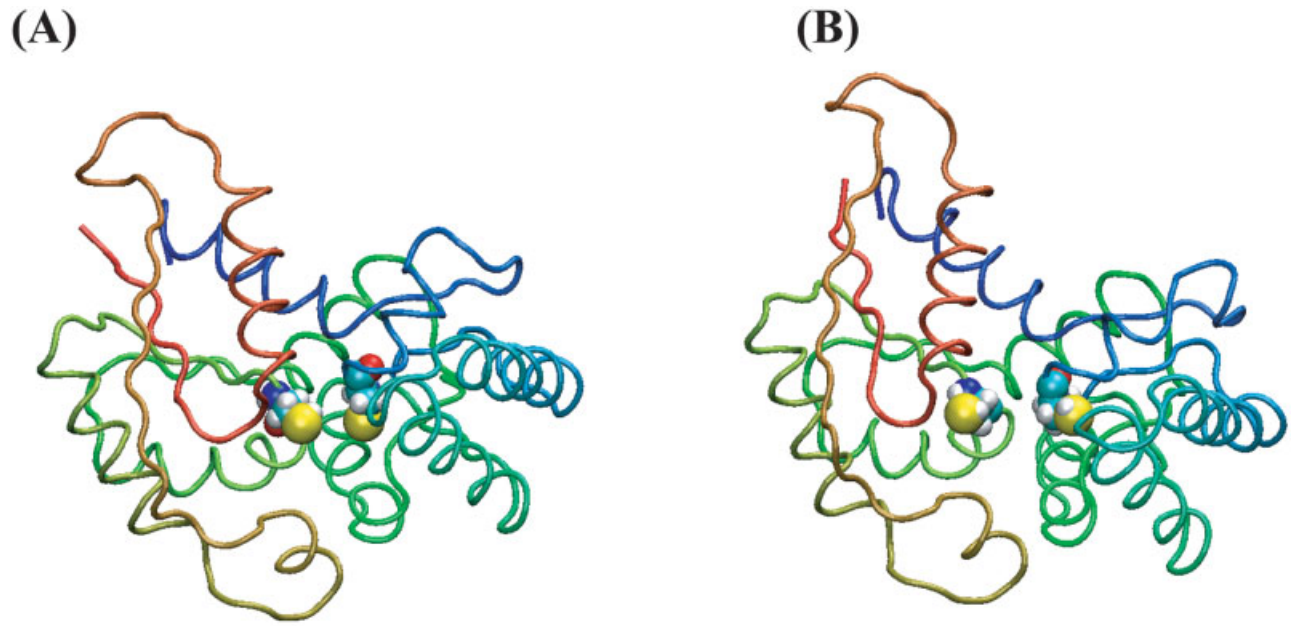

Fig. 4. Schematic drawings of the PhAspR structure in the contracted and expanded states during MD simulation at 425 K. Figures are schematic drawings of the PhAspR simulated structures at 680 ps (**A**) and 940 ps (**B**) during MD simulation at 425 K, in which the distance between the catalytic cysteine residues are contracted and expanded, respectively. Two yellow spheres represent γ-sulfur atoms of cysteine residues.

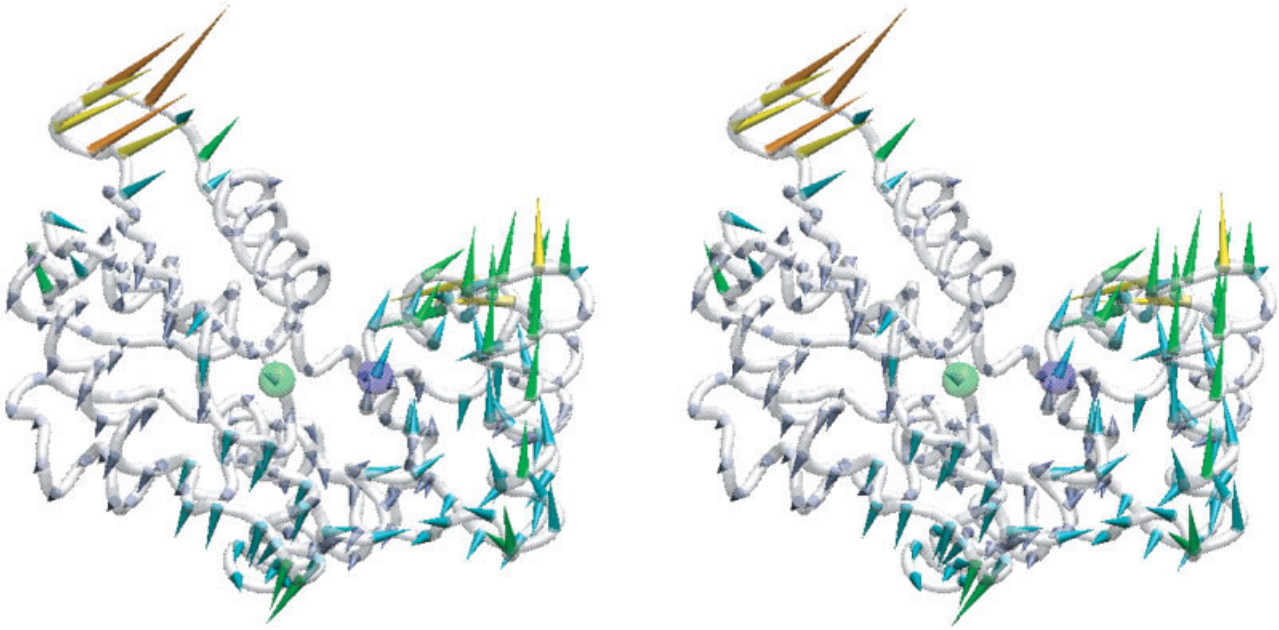

Fig. 5. Principal component analysis of the slow molecular motion at 375 K. A stereoview of the first mode, which corresponds to the slowest molecular motion, is shown using a tube model. Two α-carbon atoms in cysteine residues with the γ-sulfur atoms are represented by green (Cys82) and blue (Cys194) spheres. The color of the cones indicates the length of the eigenvector changing from orange (long) to blue (short).

the closed state, the entrance to the active site seems to be too narrow for an aspartic acid to go through. In contrast, the entrance to the active site is widely open for an aspartic acid in the open state.

This analysis implied that by changing the conformation of the dihedral angle, N-Cα-Cβ-Cγ of TYR160, PhAspR would open and close the gate of the catalytic site around the active temperature of 375 K. Thus, the opening and closing of the TYR160 gate might be related to the activation of PhAspR at elevated temperatures.

MD Simulation of the Docking of an L-Aspartic Acid into the Active Site of PhAspR

We performed simulations of the docking of the L-aspartic acid into the active site. More than 30 runs were carried out with different initial conditions, where the

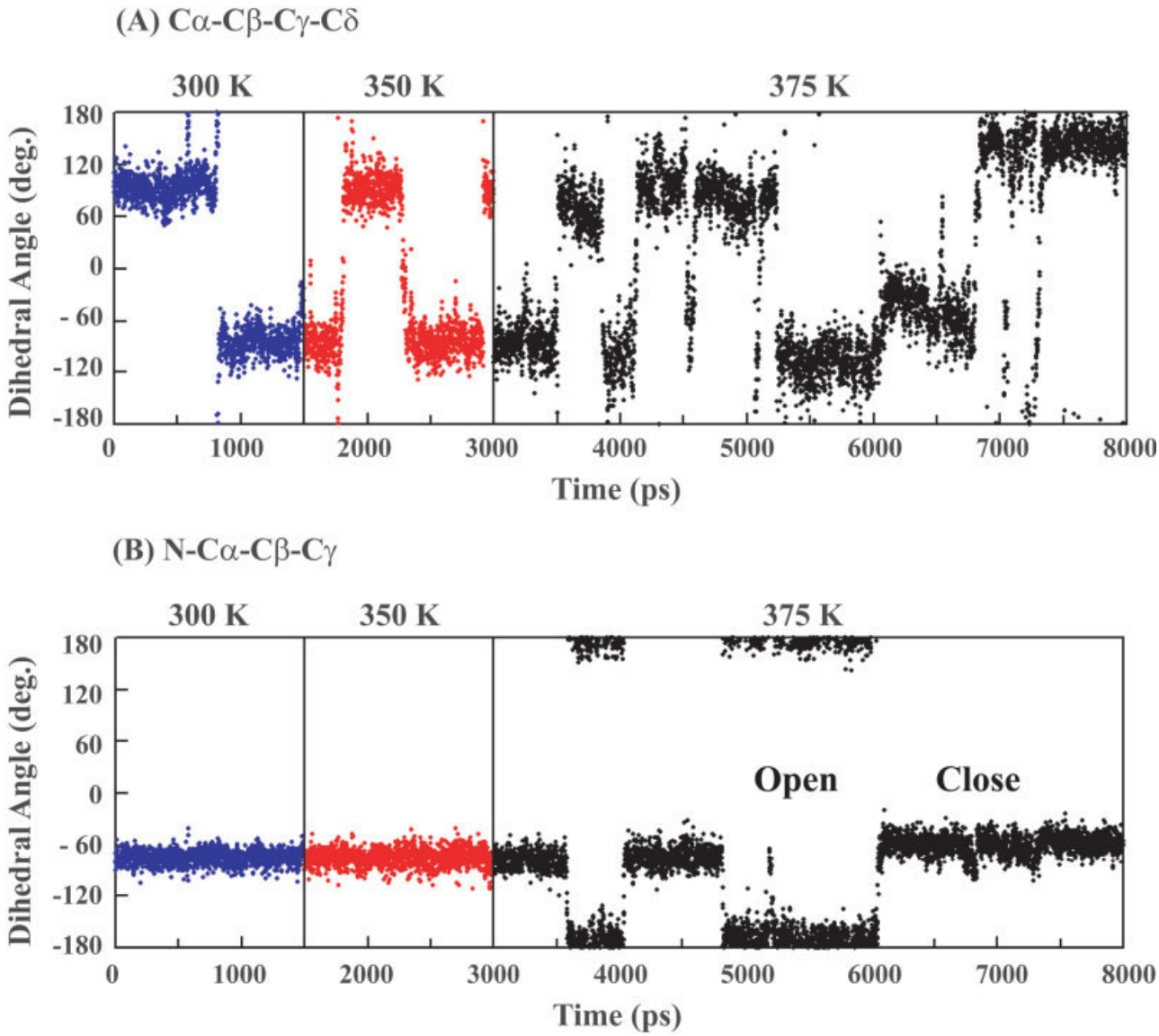

Fig. 6. Time evolution of the conformation of Tyr160 during MD simulation. The time evolutions of the dihedral angles, (**A**) Cα-Cβ-Cγ-Cδ and (**B**) N-Cα-Cβ-Cγ during MD simulation from 300 to 375 K are plotted. [Color figure can be viewed in the online issue, which is available at www.interscience.wiley.com.]

phenol group gate of Tys160 was initially open and the L-aspartic acid was placed 10 to 20 Å away from the sulfur atoms. The L-aspartic acid went into the active site in five runs, and we analyzed one of these runs in detail.

The time evolutions of the distances N(Lys164) to Oγ(L-aspartic acid), O(Asp47) to N(L-aspartic acid), N(Arg48) to Oγ(L-aspartic acid), S(Cys82) to Cα(L-aspartic acid), and S(Cys194) to Cα(L-aspartic acid) are shown in Figure 8. The distances S(Cys82) to Cα(L-asparitic acid), S(Cys194) to Cα(L-asparitic acid) were enlarged during the first 50 ps to ~ 20 Å, implying that the L-aspartic acid was moving above the entrance of the active site. Finally, the distances gradually shortened to around 5 Å, showing that the L-aspartic acid docked into the active site. At 60 ps, all the distances started to decrease. Among them, the distance N(Lys164) to Oγ(L-aspartic acid) suddenly decreased from 12 to 3 Å. This indicates that the electrostatic interaction with Lys164 is the first driving force for L-aspartic acid entering in the catalytic site. Then, the distances O(Asp47) to N(L-aspartic acid) and N(Arg48) to Oγ(L-aspartic acid) gradually decreased to ~ 3 Å at 160 ps, showing that the L-aspartic acid was attracted to the Asp 47 and Arg48. After 300 ps, the distances S(Cys82) to Cα(L-aspartic acid), S(Cys194) to Cα(L-aspartic acid), and N2(Arg48) to Oγ(L-aspartic acid) decreased to 3 to 6 Å. This indicates that the L-aspartic acid docked between the sulfur atoms of Cys82 and Cys194, although it was still attracted by Arg48. By contrast, the distances O(Asp47) to N(L-aspartic acid) and N(Lys164) to Oγ(L-aspartic acid) increased to 7 to 10 Å, suggesting that L-aspartic acid was detached from Asp47 and Lys164 when it docked between the sulfur atoms of Cys82 and Cys194. Thus, Asp47 and

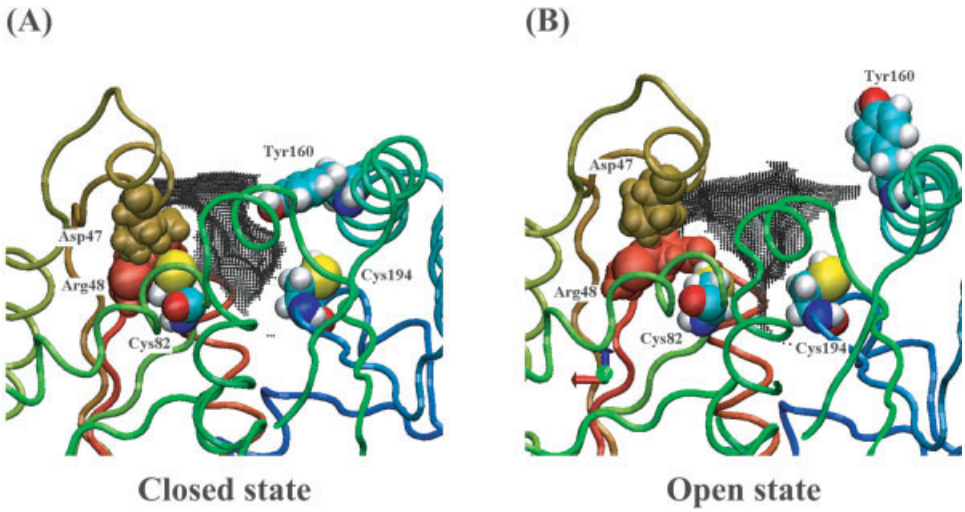

Fig. 7. Comparison of the accessible space to the catalytic site between the (**A**) closed and (**B**) open states of the Tyr160 gate. Grid points more than 1.5 Å away from the van der Waals sphere atoms of the PhAspR are plotted using black points. The backbone is drawn by tube model. Residues around the active site [Tyr160, Cys82, Cy194, Met10 (red) and Arg48 (ochre)] are drawn by van der Waals model.

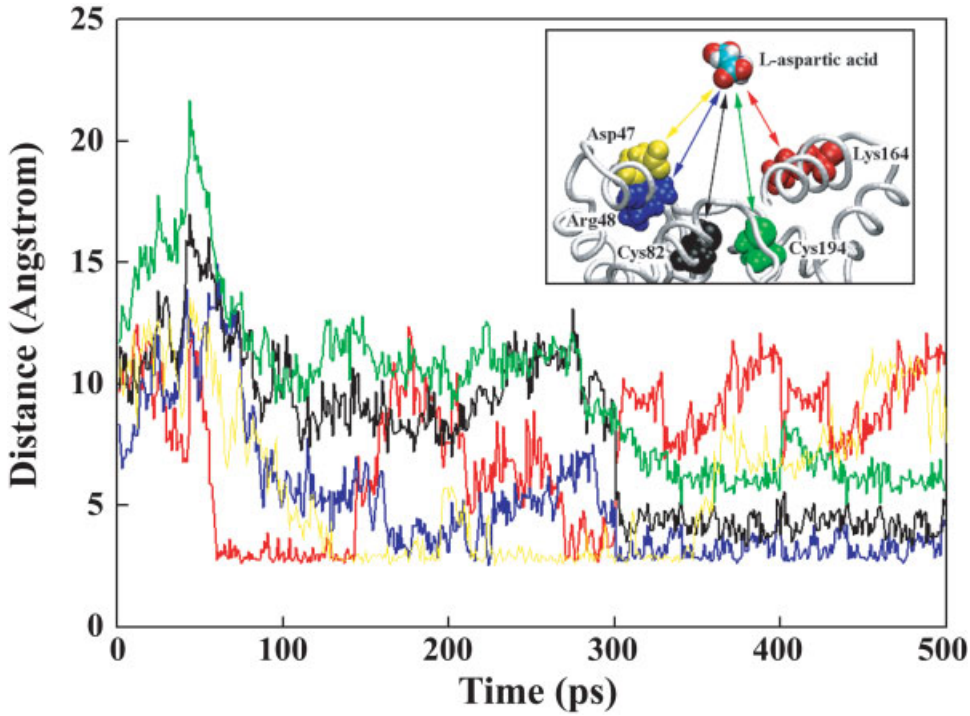

Fig. 8. Time evolutions of the distances between Cα of L-aspartic acid and atoms of residues playing important roles in the docking process. The time evolutions of the distances, N(Lys164) to Oγ(L-aspartic acid) (red), O(Asp47) to N(L-aspartic acid) (yellow), N(Arg48) to Oγ(L-aspartic acid) (blue), S(Cys82) to Cα(L-aspartic acid) (black), and S(Cys194) to Cα(L-aspartic acid) (green), from 0 to 8000 ps are plotted. The arrows in the inset represent the pairs of atoms using the same colors with the plots mentioned above.

Lys164 do not contribute to keeping the L-aspartic acid docked in the active site.

From the MD simulations we obtained information on the docking of L-aspartic acid into PhAspR (Fig. 9). At first, the L-aspartic acid approaches the entrance of the active site through diffusion and the electrostatic attractive force of Asp47, Arg48, and Lys164 [Fig. 9(A)]. Then, it is captured by Lys164 [Fig. 9(B)]. Because Lys164 is expected to be highly mobile due to its configuration, the L-aspartic acid can readily move around the entrance to be trapped by Asp47 and Arg48 [Fig. 9(C)], whose motion is restricted by steric hindrance from the surrounding residues. Finally, the L-aspartic acid docks between the sulfur atoms with an oxygen atom stabilized by Arg48 [Fig. 9(D)].

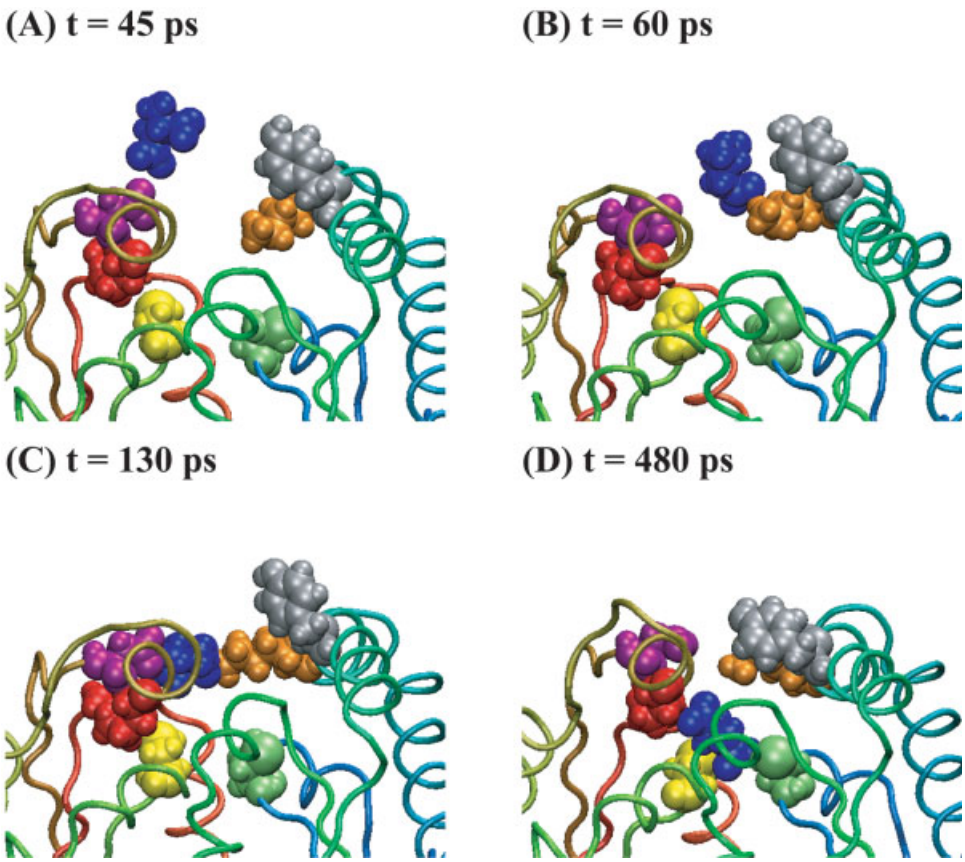

Fig. 9. Docking process of L-aspartic acid into the catalytic site of PhAspR. Schematic drawings for the position of the L-aspartic acid and the conformation of the catalytic site of PhAspR at 45 ps (**A**), 60 ps (**B**), 130 ps (**C**), and 480 ps during the docking MD simulation are shown. The backbone is shown by tube model. L-aspartic acid (blue) and the important residues around the catalytic site, Asp47 (purple), Arg48 (red), Lys164 (orange), Tyr160 (gray), Cys82 (yellow), and Cys194 (green), are drawn by van der Waals model.

DISCUSSION

Because the crystal structure of PhAspR showed that the two catalytic cysteine residues are separated from each other and also the entrance of the catalytic site is closed, it was impossible to elucidate the reaction mechanism of aspartate racemase. MD simulation in this study provided clues to solve this problem. At an elevated temperature, the distance between the two active γ-sulfur atoms of the cysteine residues oscillated to become periodically shorter than the predicted cooperative distance for racemization at high temperature. The conformation of Tyr160, which is located at the entrance of the cleft and inhibits the entry of a substrate, also changed periodically to open the entrance at 375 K. These conformational changes at elevated temperatures coincide well with the activation of PhAspR at high temperature.

The MD simulation of glutamate racemase has been performed.[35] The active site of glutamate racemase displayed an unusual flexibility in substrate ligation, and several transitions between stable binding patterns were observed. Oscillation of the distance between the catalytic cysteines and α-carbon of the substrate analogue was also observed at 358 K. The change correlates with the changes of the dihedral angles, χ_S and χ_{SH} of Cys178.

One of the catalytically important amino acid residues, Lys164, was found to be close to Tyr160. Detailed analysis of the MD simulation shows that the conformational change of Tyr160 at high temperature is likely to be related with Lys164. Mutations of Lys164 to Arg, Leu, and Ala resulted in a significant decrease in catalytic activity. Among them, mutation to Ala resulted in the lowest level of activity. By contrast, K164L exhibited the highest level of activity even though the positive charge is important for binding with substrate as shown in the docking simulation. Thus, a bulky side chain at 164th amino acid is required to change the conformation of Tyr160 to open the entrance of the catalytic site.

In the docking MD simulation, the spontaneous entrance of the substrate L-aspartic acid molecule into the catalytic site was observed. The driving force for this is the electrostatic interaction with Asp47, Arg48, and Lys164. The highly mobile Lys164 first attracts the aspartic acid via electrostatic attractive force and then transfers it to Asp47 and Arg48. The less mobile Arg48 attracts the aspartic acid also using electrostatic attractive force and holds it until it docks between the sulfur atoms of Cys82 and Cys194. At the same time, Asp47 attracts the aspartic acid to regulate its orientation for docking into the active site. Interestingly, both

mutants R48K and K164R have very weak activity compared with the wild type even though the positive charge is conserved. Thus, the role of these conserved positively charged residues is not only to attract the aspartic acid to the catalytic site but also to position the substrate.

ACKNOWLEDGMENT

We sincerely thank Professor Hiroshi Homma and Dr. Masae Sekine for supporting the analysis of aspartic acid enantiomers by HPLC. We also appreciate Mr. Toshiro Shimada of Fuji Xerox Co., Ltd., for fruitful discussion and support. The work reported here is a part of the 21st Century COE (Center of Excellence) program of the Future Nano-Materials research and education project, which is financially supported by the Ministry of Education, Science, Sports, Culture, and Technology through Tokyo University of Agriculture & Technology. This work was also supported by a grant of the National Project on Protein Structural and Functional Analyses from the Ministry of Education, Science, Sports and Culture of Japan to MY.

REFERENCES

1. Matsumoto M, Homma H, Long Z, Imai K, Iida T, Maruyama T, Aikawa Y, Endo I, Yohda M. Occurrence of free D-amino acids and aspartate racemases in hyperthermophilic archaea. J Bacteriol 1999;181:6560–6563.
2. Watanabe T, Shibata K, Kera Y, Yamada R. Occurrence of free D-aspartate and aspartate racemase in the blood shell *Scapharca broughtonii*. Amino Acids 1998;14:353–360.
3. Chouinard ML, Gaitan D, Wood PL. Presence of the N-methyl-D-aspartate-associated glycine receptor agonist, D-serine, in human temporal cortex: comparison of normal, Parkinson, and Alzheimer tissues. J Neurochem 1993;61:1561–1564.
4. Stevens ER, Esguerra M, Kim PM, Newman EA, Snyder SH, Zahs KR, Miller RF. D-serine and serine racemase are present in the vertebrate retina and contribute to the physiological activation of NMDA receptors. Proc Natl Acad Sci U S A 2003;100:6789–6794.
5. Shibata K, Watanabe T, Yoshikawa H, Abe K, Takahashi S, Kera Y, Yamada RH. Purification and characterization of aspartate racemase from the bivalve mollusk *Scapharca broughtonii*. Comp Biochem Physiol B Biochem Mol Biol 2003;134:307–314.
6. Gerlt JA, Kenyon GL, Kozarich JW, Neidhart DJ, Petsko GA, Powers VM. Mandelate racemase and class-related enzymes. Current Opin Struct Biol 1992;2:736–742.
7. Soda K, Esaki N. Pyridoxal enzymes acting on D-amino acids. Pure Appl Chem 1994;66:709–714.
8. Nakajima N, Tanizawa K, Tanaka H, Soda K. Cloning and expression in *Escherichia coli* of the glutamate racemase gene from *Pediococcus pentosaceus*. Agric Biol Chem 1986;50:2823–2830.
9. Gallo KA, Tanner ME, Knowles JR. Mechanism of the reaction catalyzed by glutamate racemase. Biochemistry 1993;32:3991–3997.
10. Tanner ME, Gallo KA, Knowles JR. Isotope effects and the identification of catalytic residues in the reaction catalyzed by glutamate racemase. Biochemistry 1993;32:3998–4006.
11. Koo CW, Blanchard JS. Chemical mechanism of *Haemophilus influenzae* diaminopimelate epimerase. Biochemistry 1999;38:4416–4422.
12. Fisher LM, Belasco JG, Bruice TW, Albery WJ, Knowles JR. Energetics of proline racemase: transition-state fractionation factors for the two protons involved in the catalytic steps. Biochemistry 1986;25:2543–2551.
13. Yamauchi T, Choi SY, Okada H, Yohda M, Kumagai H, Esaki N, Soda K. Properties of aspartate racemase, a pyridoxal 5′-phosphate-independent amino acid racemase. J Biol Chem 1992;267:18361–18364.
14. Liu L, Iwata K, Kita A, Kawarabayasi Y, Yohda M, Miki K. Crystal structure of aspartate racemase from *Pyrococcus horikoshii* OT3 and its implications for molecular mechanism of PLP-independent racemization. J Mol Biol 2002;319:479–489.
15. Liu L, Iwata K, Yohda M, Miki K. Structural insight into gene duplication, gene fusion and domain swapping in the evolution of PLP-independent amino acid racemases. FEBS Lett 2002;528:114–118.
16. Schowen KB, Limbach HH, Denisov GS, Schowen RL. Hydrogen bonds and proton transfer in general-catalytic transition-state stabilization in enzyme catalysis. Biochim Biophys Acta 2000;1458:43–62.
17. Gregoret LM, Rader SD, Fletterick RJ, Cohen FE. Hydrogen bonds involving sulfur atoms in proteins. Proteins 1991;9:99–107.
18. Hwang KY, Cho CS, Kim SS, Sung HC, Yu YG, Cho Y. Structure and mechanism of glutamate racemase from *Aquifex pyrophilus*. Nat Struct Biol 1999;6:422–426.
19. Sakuraba H, Satomura T, Kawakami R, Yamamoto S, Kawarabayasi Y, Kikuchi H, Ohshima T. L-aspartate oxidase is present in the anaerobic hyperthermophilic archaeon *Pyrococcus horikoshii* OT-3: characteristics and role in the de novo biosynthesis of nicotinamide adenine dinucleotide proposed by genome sequencing. Extremophiles 2002;6:275–281.
20. Liu L, Iwata K, Kawarabayasi Y, Kikuchi H, Kita A, Yohda M, Miki K. Crystallization and preliminary X-ray analysis of aspartate racemase from *Pyrococcus horikoshii* OT3. Acta Crystallogr D Biol Crystallogr 2001;57:1674–1676.
21. Long Z, Lee JA, Okamoto T, Sekine M, Nimura N, Imai K, Yohda M, Maruyama T, Sumi M, Kamo N, Yamagishi A, Oshima T, Homma H. Occurrence of D-amino acids and a pyridoxal 5′-phosphate-dependent aspartate racemase in the acidothermophilic archaeon, *Thermoplasma acidophilum*. Biochem Biophys Res Commun 2001;281:317–321.
22. Case D, Pearlman D, Caldwell J, Cheatham III T, Ross W, Simmerling C, Darden T, Merz K, Stanton R, Cheng A, Vincent J, Crowley M, Ferguson D, Radmer R, Seibel G, Singh U, Weiner P, Kollman P. AMBER 6. San Francisco: University of California; 2000.
23. Cornell WD, Cieplak P, Bayly CI, Gould IR, Merz KM, Ferguson DM, Spellmeyer DC, Fox T, Caldwell JW, Kollman PA. A 2nd generation force-field for the simulation of proteins, nucleic acids, and organic molecules. J Am Chem Soc 1995;117:5179–5197.
24. Kollman P, Dixon R, Cornell W, Fox T, Chipot C, Phorille A. The development/application of a 'minimalist' organic/biochemical molecular mechanic force field using a combination of ab initio calculations and experimental data. In: A. W, P. W, W. vG, editors. Computer simulation of biomolecular systems. New York: Elsevier; 1997. p 83–96.
25. Jorgensen W, Chandrasekhar J, Madura J, Klein M. Comparison of simple potential functions for simulating liquid water. J Chem Phys 1983;79:926–935.
26. Amisaki T, Toyoda S, Miyagawa H, Kitamura K. Two algorithms designed for realizing efficient combination of fast multipole method and dedicated hardware for molecular dynamics simulations. J Comput Chem 2002;1:73–82.
27. Humphrey W, Dalke A, Schulten K. VMD: visual molecular dynamics. J Mol Graphics 1996;14:33–38.
28. Cheatham TE, Miller JL, Fox T, Darden TA, Kollman PA. Molecular-dynamics simulations on solvated biomolecular systems — the particle mesh Ewald method leads to stable trajectories of DNA, RNA, and proteins. J Am Chem Soc 1995;117:4193–4194.
29. York DM, Yang WT, Lee H, Darden T, Pedersen LG. Toward the aaccurate modeling of DNA — the importance of long-range electrostatics. J Am Chem Soc 1995;117:5001–5002.
30. Ryckaert J, Ciccotti G, Berendsen H. Numerical integration of the cartesian equations of motion of a system with constraints: molecular dynamics of n-alkanes. J Comput Phys 1977;23:327–341.
31. Berendsen H, Postma J, van Grensteren W, DiNola A, Haak J. Molecular dynamics with coupling to an external bath. J Chem Phys 1984;81:3684–3690.
32. Go N. A theorem on amplitudes of thermal atomic fluctuations in large molecules assuming specific conformations calculated by normal mode analysis. Biophys Chem 1990;35:105–112.
33. Kitao A, Hirata F, Go N. The effects of solvent on the conformation and the collective motions of protein: normal mode analysis and molecular dynamics simulations of melittin in water and in vacuum. Chem Phys 1991;158:447–472.
34. Brooks BR, Janezic D, Karplus M. Harmonic-analysis of large systems .1. Methodology. J Comput Chem 1995;16:1522–1542.
35. Mobitz H, Bruice TC. Multiple substrate binding states and chiral recognition in cofactor-independent glutamate racemase: a molecular dynamics study. Biochemistry 2004;43:9685–9694.